Core nucleus polarization in Λ hypernuclei

Q. N. Usmani,[1,*] A. R. Bodmer,[2] and Z. Sauli[3]
[1]*Institute of Engineering Mathematics, University Malaysia Perlis, Malaysia*
[2]*Department of Physics, University of Illinois at Chicago, Chicago, Illinois, USA*
[3]*School of Microelectronics Engineering, University Malaysia Perlis, Malaysia*
(Received 14 March 2007; revised manuscript received 15 January 2008; published 28 March 2008)

The response of the core nucleus to the Λ in a hypernucleus is studied with a local density approximation. This reproduces the energies and radii of the core nuclei as well as the Λ-single particle (s.p.) energies quite well. The polarizing effect of the Λ depends on the core response through an "effective" compression modulus K_A of the nucleus. For a certain class of energy functional, K_A is found to be almost independent of the compression modulus K of the infinite nuclear matter. This indeed is a surprising result, and varies with the Hartree-Fock calculations with effective interactions. Reasons for this discrepancy are carefully examined. We consider values of K in the range ≈100–400 MeV. Furthermore, the polarizing effects also depend critically on $D(\rho)$, the Λ binding in nuclear matter at density ρ. For only a direct ΛN force: $D \propto \rho$ and the core nucleus contracts giving rise to relatively larger core polarization. However, for a "saturating" $D(\rho)$ (with a maximum at $\rho_m < \rho_0$, where ρ_0 is the nuclear matter equilibrium density), which is required to fit the s.p. data, the *s*-shell hypernuclei binding energies and the low energy Λp scattering data, which results from a ΛN force (including exchange) and ΛNN forces, there may be an expansion of the nucleus with nucleons flowing from the interior to the surface. This is shown to reduce the core polarization effects substantially (for ρ_m in the neighborhood of ρ_0). The resulting changes in root mean square radius and core energy depend on A, but are mostly very small, justifying their general neglect.

DOI: 10.1103/PhysRevC.77.034312 PACS number(s): 21.80.+a, 21.10.Dr, 21.65.−f, 13.75.Ev

I. INTRODUCTION

The theoretical study of hypernuclei has focused strongly on learning about the strong and weak hyperon-nuclear interactions [1–3]. In particular, we have some reasonable knowledge of the strong ΛN, ΛNN, and $\Lambda\Lambda$ forces [4–10], although there is much more to be learned. However, there has been a long expressed hope that if the hyperon-nuclear interaction is reasonably well known, one may use the hyperon, in particular the Λ, to probe the structure of core nuclei. This hope arises from the consideration that the Λ, being distinguishable, can occupy any state in the nucleus. Also, the lifetime of Λ-hypernuclei is of the order of 10^{-10} s, these systems can then be regarded as stable on the strong nuclear time scale. Thus one may address such questions as the effect of Λ on the moment of inertia and on rotational bands of the core nucleus, and in general consider the response of nuclei to the presence of a Λ. It may also be possible in the future that Λ single particle energies in higher angular momentum states in heavy nuclei may yield some information about nuclear surface properties. In the present work, we study the effect of a Λ on spherical core nuclei. In particular, we calculate the changes in binding energy (core polarization energy) and of the root mean square (rms) radii of the core nuclei due to presence of the Λ.

The presence of a Λ in hypernucleus causes a compression or dilation of the core nucleus depending upon the nature of the Λ-nuclear interactions [11–15]. The relationship between the incompressibility and the change in the core size as well as the polarization energy due to presence of Λ has been extensively studied mainly within the Hartree-Fock approximation using Skyrme and finite range effective interactions [11–21]. A few studies pertain to model calculations [11,22] based upon qualitative considerations. The polarization energies are found to be 0.1 to 1.2 MeV in the range $16 \leqslant A \leqslant 40$ and increases or stays constant with respect to A at least within this range [11,16]. The core polarization energies have also been found to decrease as K increases. In the case of ${}^{16}_{\Lambda}$O, it was found to increase with K [21]. However, these values of core polarization energies are not small and secondly to our knowledge they are mostly confined to light and medium A nuclei. It was demonstrated in [7] that for ${}^{6}_{\Lambda\Lambda}$He, the core polarization effect magnifies in double hypernuclei where the polarization energies increase roughly by a factor of 3 or more (also see [21,23]). Their inclusion assumes importance in cluster model calculations where in a few cases a rigid core approximation has been used. For a consistent treatment of hypernuclei it is thus desirable that we study core polarization in greater detail. The only empirical knowledge about core-polarization comes from a γ transition and is limited to contraction of the ^{6}Li core nucleus in ${}^{7}_{\Lambda}$Li [24]. But this represents a very special situation where the Λ probably shrinks the rms radius of the loosely bound *p*-shell nucleons by a large amount. We shall very briefly comment on this at a later stage.

In the present study, we develop an extended Thomas-Fermi theory using a local density approach ("Thomas-Fermi" model for short) for nuclei and hypernuclei and demonstrate that for "realistic" Λ-nuclear interactions, the core polarization effects are in general very small, both the polarizing energies as well as the change in rms radii. The smallness of the core polarization effects on radii was also pointed out by Rayet [15] who inferred that presence of a repulsive three-body ΛNN

*Corresponding author: qamar@unimap.edu.my

force may turn a contraction into dilation for ${}^{16}_{\Lambda}$O. A dilation of the core nucleus in presence of Λ has also been found by Lanskoy [11], but in most of the studies contraction is a preferred conclusion [11–24].

For a direct ΛN interaction, our results are in line with earlier studies. However, there are important major differences. We find that the behavior of the core polarization depends upon an "effective compression modulus," K_A (to be defined later) of a particular nucleus and on the structure of nuclear surface. It does not depend directly on the compression modulus K of infinite nuclear matter. K_A is commonly used in the calculation of the energies of the giant monopole resonances which correspond to the "breathing mode" of the nucleus [25]. Our nuclear Hamiltonian, or the energy density functional does not depend on a Skyrme or any other NN interaction, but is rather determined by expanding the energy per nucleon of nuclear matter around the equilibrium density by means of Taylor series and then adopting a purely phenomenological approach. In particular, we find that for a certain class of energy functional, K_A depends on the compression modulus K of the infinite nuclear matter rather weekly and decreases gradually with increasing K in the range 100 to 300 MeV and then starts rising slowly. This indeed is a surprising result. Thus the relationship between the compressibility and the polarization of the core nucleus is not as simple as one might have expected it form the earlier Hartree-Fock studies which employ either zero-range Skyrme or finite range effective interactions. In the Hartree-Fock scheme K_A is found to be proportional to K [25,26] and has a strong dependence on it. We discuss in detail the reasons for this paradox by partially emulating finite range as well as the zero range Skyrme interactions with in our formalism.

We take into account the differences between the neutron and proton densities explicitly arising out of the neutron-proton imbalance and the presence of Coulomb forces in nuclei. The nuclei (hypernuclei) considered range from ^{10}B ($^{11}_{\Lambda}$B) to ^{243}Am ($^{244}_{\Lambda}$Am), a total of 32 nuclei. Our local density approach gives a good description of the static properties of nuclei and hypernuclei, such as the binding energies and rms radii. The approach uses the variational principle which minimizes the energy of the nucleus (hypernucleus) with respect to changes in neutron and proton densities. Thus rms charge radii, nuclear surface diffuseness, total binding energies and other nuclear properties are an outcome of the theory.

The energy of the hypernucleus is the sum of the energy of the core nucleus and that of the Λ:

$$ {}^{A}_{\Lambda}E[\rho] = {}^{A-1}\hat{E}[\rho] + E_{\Lambda}[\rho], \tag{1.1} $$

where ρ is the density of the core nucleus; $E_{\Lambda}[\rho]$ is the sum of the kinetic and potential energies of the Λ moving in the potential generated by the Λ-nuclear interactions. ${}^{A-1}\hat{E}[\rho]({}^{A-1}E[\rho])$ is the energy of the nucleus in the presence (absence) of the Λ. The square brackets indicate that the energies are functional of ρ. The calculation of ${}^{A-1}E[\rho]$ is described in Sec. II, and that of $E_{\Lambda}[\rho]$ (with the Λ in $\ell \leqslant$ 4 states) is described in Refs. [9,27,28] and briefly in Sec. III. In Sec. III we also describe the calculation of ${}^{A}_{\Lambda}E[\rho]$ including the polarizing effect of the Λ. Section IV presents and discusses our results for the polarizing energy and related questions. Section V is conclusions.

II. THOMAS-FERMI MODEL OF THE NUCLEUS

A. The model

Our model is phenomenological and generally has been in use for a long time (e.g., Refs. [29–32] for early version and Refs. [33,34] for more recent elaborate versions). For our purposes our model gives a good description of nuclei and adequately describes the nuclear response of the Λ.

The energy ${}^{A-1}\hat{E}[\rho]$ or ${}^{A-1}E[\rho]$ is an integral of an energy density which accounts for the volume, surface, asymmetry energies plus coulomb and pairing terms:

$$ \begin{aligned} {}^{A-1}E[\rho] = \int \Bigg[& \varepsilon(\rho) + \frac{\hbar^2}{72m}\left(\frac{\nabla\rho}{\rho}\right)^2 + \frac{\hbar^2}{6m}\frac{\nabla^2\rho}{\rho} + a_{\rho}\frac{(\nabla\rho)^2}{\rho} \\ & + a_{\rm sym}(\rho)\left(\frac{\rho_n - \rho_p}{\rho}\right)^2 \Bigg] \rho d\vec{r} + \text{Coulomb} \\ & + \text{Pairing}, \end{aligned} \tag{2.1} $$

where $\rho_n(r)$ and $\rho_p(r)$ are respectively the neutron and proton densities, and $\rho(r)$ is the total nucleon density; $\rho(r) = \rho_n(r) + \rho_p(r)$. We ignore shell and deformation effects which have little relevance for the present investigation. In expression (2.1), the term $\varepsilon(\rho)$ represents the equation of state of symmetric nuclear matter, i.e., the binding energy per nucleon as a function of nuclear matter density. The terms $(\nabla\rho)^2/\rho$ and $(\nabla\rho)^2/\rho^2$are essential for the surface properties. To a very good approximation $a_{\rm sym}(\rho)$ can be considered as independent of ρ [35]. The parameters $a_{\rm sym}$ and a_{ρ} are determined by fitting ${}^{A-1}E$ to the experimental binding energies and rms radii of nuclei as described later. For the coulomb energy we use

$$ \begin{aligned} \text{Coulomb} = & \frac{1}{2}e^2 \int \frac{\rho_p(\vec{r}_1)\rho_p(\vec{r}_2)}{|\vec{r}_1 - \vec{r}_2|} d\vec{r}_1 d\vec{r}_2 \\ & - \frac{3}{4}\left(\frac{3}{\pi}\right)^{1/3} e^2 \int \rho_p^{4/3}(r) d\vec{r}, \end{aligned} \tag{2.2} $$

where the second term on the right-hand side (r.h.s.) is an approximation to the exchange part of the coulomb energy. For the pairing term we employ

$$ \text{Pairing} = -a_{\rm pair}\frac{(-1)^Z + (-1)^N}{(N+Z)^{3/4}}. \tag{2.3} $$

Though, we have included the small pairing energy term, but it is not expected to play significant role in the present study.

For $\varepsilon(\rho)$ in Eq. (2.1) one may utilize a functional from the results of nuclear matter calculations using some effective interaction like Skyrme [36] or Gogny [37] types, or the one which imitates a realistic Hamiltonian [38–41]. However, this ties us to a specific form of the interaction. Therefore, in the present study, we adopt a more general approach in which the different values of the parameters of $\varepsilon(\rho)$ could possibly emulate, at least partly, the various diverse interactions. Making a Taylor series expansion of $\varepsilon(\rho)$ around $\rho = \rho_0$, and

since at saturation $d\varepsilon/d\rho|_{\rho_0} = 0$, leads to the following ansatz:

$$\varepsilon(\rho_{\geqslant}) = -u_v + \frac{K}{18}\left(\frac{\rho-\rho_0}{\rho_0}\right)^2 + M\left(\frac{\rho-\rho_0}{\rho_0}\right)^3, \quad \text{for} \quad \rho \geqslant \rho_x \tag{2.4a}$$

$$\varepsilon(\rho_{\leqslant}) = A\rho + B\rho^2 + C\rho^3 + D\rho^4 + \frac{3\hbar^2(3\pi^2)^{2/3}}{10\,m_N\rho}\left(\rho_n^{5/3} + \rho_p^{5/3}\right). \quad \text{for} \quad \rho \leqslant \rho_x. \tag{2.4b}$$

In Eq. (2.4a), the parameter M is a measure of deviation from parabola in the vicinity of the saturation density ρ_0, which is related to an asymmetry in the saturation curve. We may have an idea of the values of M from the calculation of nuclear matter equation of state using realistic Hamiltonians [38–41]. Higher densities $\rho > 0.20$ fm^{-3} are irrelevant in the present study as they are not accessible by normal nuclei or hypernuclei. Thus the values of M generally refer to low values of ρ. The density ρ_x is a parameter between 0 and ρ_0 to be determined as described later. The terms containing $\rho^{5/3}$are the neutron and proton single particle kinetic energies.

We now impose the conditions that at $\rho = \rho_x$

$$\varepsilon(\rho_{\leqslant}) = \varepsilon(\rho_{\geqslant}), \tag{2.5a}$$

$$\frac{\partial\varepsilon(\rho_{\leqslant})}{\partial\rho} = \frac{\partial\varepsilon(\rho_{\geqslant})}{\partial\rho}, \tag{2.5b}$$

$$\frac{\partial^2\varepsilon(\rho_{\leqslant})}{\partial\rho^2} = \frac{\partial^2\varepsilon(\rho_{\geqslant})}{\partial\rho^2}, \tag{2.5c}$$

$$\frac{\partial^3\varepsilon(\rho_{\leqslant})}{\partial\rho^3} = \frac{\partial^3\varepsilon(\rho_{\geqslant})}{\partial\rho^3}, \tag{2.5d}$$

where $\rho_{\leqslant}(\rho_{\geqslant})$ means ρ less (greater) than or equal to ρ_x . The conditions of Eq. (2.5) fix the parameters A, B, C, and D of Eq. (2.4b) in terms of ρ_x , the volume term u_v, the compression modulus K and the parameter M appearing in Eq. (2.4a). This guarantees that $\varepsilon(\rho)$ and it's derivatives are well behaved as one would expect from the nuclear matter calculations with Skyrme or other effective interactions. Continuity up to third derivative in Eq. (2.5) ensures that the analogue of the "compression modulus" in the surface region is continuous. The condition (2.5d), though not essential, shall be needed to appreciate the influence of K at lower densities.

For the volume term u_v and the equilibrium density ρ_0 we use 16.0 MeV and 0.16 fm^{-3}, respectively, which is now an accepted norm. We also consider other values of u_v and ρ_0 in order to mimic at least partially the Skyrme, Gogny, and other effective interactions. For K, we use five values, namely, 100, 200, 250, 300, and 400 MeV, in order to explore the dependence on K of the changes of the core in the presence of the Λ. However, the detailed results are only presented for the range of K between 200 and 300 MeV as the realistic values of K lie between 230–270 MeV [42].

For the variational neutron (proton) densities, we use a two parameter Fermi distribution:

$$\rho_{n(p)}(r) = \frac{N_{n(p)}}{1 + \exp((r - R_{n(p)})/t_{n(p)})}, \tag{2.6}$$

where $R_{n(p)}$ and $t_{n(p)}$ are the radius and the surface thickness parameters for neutrons and protons, respectively. Therefore, for each nucleus we have four variational parameters to be varied. These are determined by minimizing the energy. $N_{n(p)}$ is the normalization constants for the neutrons and protons given by

$$N_{n(p)} = \frac{3N(Z)}{4\pi R^3}\left[1 + \frac{\pi^2 t_{n(p)}^2}{R_{n(p)}^2}\right]^{-1}, \tag{2.7}$$

where $N$and$Z$ are the total number of neutrons and protons, respectively.

A useful quantity of interest is the effective compression modulus widely used in connection with the giant monopole resonances. This is defined by [25,26]

$$K_A = 4\eta_0^2 \frac{d^2(E/A)}{d\eta^2}\bigg|_{\eta_0} = \xi_0^2 \frac{d^2(E/A)}{d\xi^2}\bigg|_{\xi_0}, \tag{2.8}$$

where $\eta_0 = \langle r^2\rangle_0/A$, $\xi_0^2 = \langle r^2\rangle_0/A$, and $\langle r^2\rangle_0$ is the mean square radius of matter distribution and is given by

$$\langle r^2\rangle_0 = N\langle r^2\rangle_{0n} + Z\langle r^2\rangle_{0p}, \tag{2.9}$$

where $\langle r^2\rangle_{0n}$ and $\langle r^2\rangle_{0p}$ are the single particle neutron and proton mean square radii, respectively:

$$\langle r^2\rangle_{0n(p)} = \tfrac{3}{5}\left(R_{n(p)}^2 + \tfrac{7}{3}\pi^2 t_{n(p)}^2\right) \tag{2.10}$$

K_A is calculated using scaling [43] approximation or putting constraint on the rms radii as in the Hartree-Fock approach [25,26]. These are specific to monopole excitations in the giant resonances. In this study we shall use the scaling method in a more general form to calculate K_A [44]. Some details regarding these calculations are given below. Details about scaling are given in the next subsection.

With the help of Eqs. (2.9) and (2.10), the functional derivative in Eq. (2.8) can be carried out:

$$\frac{d^2(E/A)}{d\eta^2}\bigg|_{\eta_0} = \frac{E(\langle r^2\rangle_0 + \delta\langle r^2\rangle) + E(\langle r^2\rangle_0 - \delta\langle r^2\rangle) - 2E(\langle r^2\rangle)}{(\delta\langle r^2\rangle)^2} \tag{2.11}$$

with $\delta\langle r^2\rangle \to 0$. The change in the mean square radius can be calculated from

$$\delta\langle r^2\rangle = \sum_{i=n(p)} \frac{3}{5} X_i \left[2R_i\delta R_i + \frac{7}{3}\pi^2 2t_i\delta t_i\right], \tag{2.12}$$

where $X_i = N$ or Z for $i = n$ or p. Therefore

$$\langle r^2\rangle_0 \pm \delta\langle r^2\rangle = \sum_{i=n(p)} \frac{3}{5} X_i \left[R_i^2\left(1 \pm \frac{2\delta R_i}{R_i}\right) + \frac{7}{3}\pi^2 t_i^2\left(1 \pm \frac{2\delta t_i}{t_i}\right)\right]. \tag{2.13}$$

For small δR_i and δt_i, Eq. (2.13) can be written as

$$\langle r^2\rangle_0 \pm \delta\langle r^2\rangle = \sum_{i=n(p)} \frac{3}{5} X_i \left[(R_i \pm \delta R_i)^2 + \frac{7}{3}\pi^2 (t_i \pm \delta t_i)^2 \right]. \quad (2.14)$$

Thus for small changes, changing $R_i \to R_i \pm \delta R_i$ and $t_i \to t_i \pm \delta t_i$ in the expression for $\langle r^2\rangle_0$, we can easily calculate the r.h.s. of Eq. (2.11). These calculations shall be presented in the next subsection.

We may point out that in our calculations of energies or other quantities, the effective compression modulus K_A does not enter directly as it does in case of the calculations for energies of the giant monopole resonances. But in our case it plays an important role in understanding the paradoxical nature of some of our results.

B. Determination of nuclear parameters and results for nuclei

We have made calculations for a number of nuclei ranging from ^{10}B to ^{243}Am including all those nuclei (and in their neighborhood) for which the single-particle data on hypernuclei ($A \leqslant 208$) are available [45]. For the nuclei we calculate $^{A-1}E[\rho]$. Since the values of u_v and ρ_0 have been fixed (and are consistent with those of similar studies) we are left with five parameters ρ_x, a_ρ, $a_{\rm sym}$, $a_{\rm pair}$, and M which are determined as follows. The parameter ρ_x was varied in steps of 0.03 in the range 0.03–0.12. For a given K (i.e., 100, 200, 250, 300, or 400 MeV) and ρ_x (i.e., 0.03, 0.06, 0.09, or 0.12) and for a given choice of parameters a_ρ, $a_{\rm sym}$, $a_{\rm pair}$, and M the energy is minimized with respect to $R_{n(p)}$ and $t_{n(p)}$ for 32 nuclei. We then construct

$$\chi^2 = a \sum_{i=1}^{32} \left({}^{A-1}E_i - E_i^{\rm exp} \right)^2 + b \sum_{i=1}^{32}{}' \left(\frac{{\rm rms}_i^{\rm cal} - {\rm rms}_i^{\rm exp}}{{\rm rms}_i^{\rm exp}} \right)^2, \quad (2.15)$$

where ${\rm rms}_i$ are the calculated and experimental rms radii. The experimental values for the rms radii are taken from Refs. [46,47] and for the experimental energies from Ref. [48]. The prime on the summation sign in the second term indicates that only those values are included in the summation for which the experimental data on rms radii are available. The parameter values a and b are chosen to give suitable weights (approximately equal) to energies and rms radii, $a = 1/1600\,{\rm MeV}^{-2}$, $b = 100$. The χ^2, Eq. (2.15), is then minimized this with respect to a_ρ, $a_{\rm sym}$, $a_{\rm pair}$, and M by a standard minimization procedure. Thus for each set of a_ρ, $a_{\rm sym}$, $a_{\rm pair}$, and M the energies $^{A-1}E_i$ are minimized with respect to the parameters $R_{n(p)}$ and $t_{n(p)}$ of the density, and subsequently Eq. (2.15) is minimized with respect to a_ρ, $a_{\rm sym}$, $a_{\rm pair}$, and M. This procedure gives us a_ρ, $a_{\rm sym}$, $a_{\rm pair}$, and M, as well as $R_{n(p)}$ and $t_{n(p)}$ and thus ρ^{A-1}. The parameter values are displayed in Table I. It is seen that for $K = 100$ and 400 MeV, the absolute values for the parameter M are large. It is instructive to look at the values of M from nuclear matter calculations. For this purpose in Fig. 1 we plot the equation of state of symmetric nuclear matter for four realistic nuclear Hamiltonians corresponding to the various Urbana and Argonne two-and three-body interactions from the published results [38–41]. The curves are obtained by fitting the data to Eq. (2.4a) in the density range $0.05 \leqslant \rho \leqslant 0.30$ fm^{-3}. This gives (a) UV14+UVII: $M = 0.276$ MeV, $K = 200.7$ MeV, $\rho_0 = 0.175$ fm^{-3}; (b) AV14+UVII: $M = 0.343$ MeV, $K = 206.2$ MeV, $\rho_0 = 0.196$ fm^{-3}; (c) UV14+TNI: $M = -4.337$ MeV, $K = 263.5$ MeV, $\rho_0 = 0.159$ fm^{-3}; (d) V18+UIX*+Relativistic and other Corrections: $M = -3.505$ MeV, $K = 257.2$ MeV, $\rho_0 = 0.159$ fm^{-3}.

TABLE I. The parameter values for various fits to binding energies and rms radii for type I energy functional. For details, see text.

K (MeV)	M (MeV)	a_ρ (MeV)	$a_{\rm sym}$ (MeV)	$a_{\rm pair}$ (MeV)	ρ_x (fm^{-3})	χ^2
100	−21.029	36.958	26.127	42.250	0.12	0.837
	−20.077	37.160	26.210	41.930	0.09	0.847
	−19.643	36.818	26.249	41.818	0.06	0.861
	−18.887	36.774	26.330	42.187	0.03	0.882
200	−7.239	39.084	25.775	41.055	0.12	0.659
	−8.207	39.449	25.770	40.506	0.09	0.650
	−8.667	39.604	25.749	40.313	0.06	0.645
	−8.675	39.742	25.757	40.201	0.03	0.644
250	−0.672	39.997	25.616	40.329	0.12	0.613
	−2.714	40.300	25.550	40.108	0.09	0.605
	−3.605	40.589	25.522	39.841	0.06	0.599
	−4.035	40.670	25.478	39.712	0.03	0.595
300	5.887	40.969	25.508	40.118	0.12	0.592
	2.700	41.061	25.396	39.752	0.09	0.584
	1.207	41.252	25.318	39.382	0.06	0.579
	0.445	41.355	25.244	39.036	0.03	0.575
400	14.815	39.460	24.828	42.887	0.12	0.689
	12.884	41.887	25.097	38.970	0.09	0.583
	10.436	42.088	24.948	38.372	0.06	0.581
	9.028	42.184	24.812	37.762	0.03	0.580

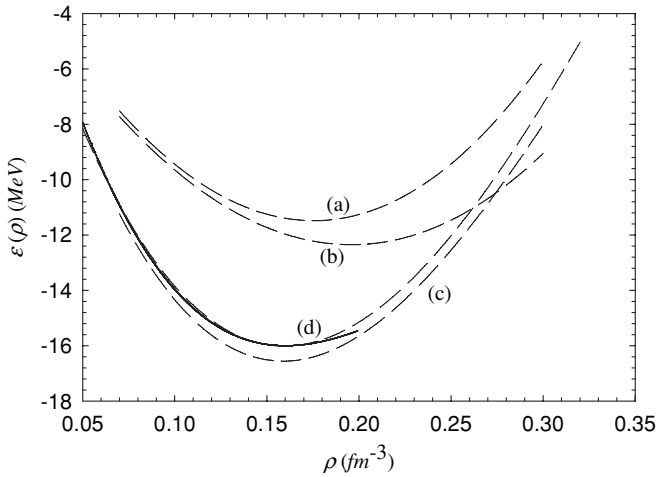

FIG. 1. Energy of nuclear matter as a function of the density ρ in fm^{-3} for four realistic Hamiltonians. See text for further explanation. The solid curve is the result of our calculations, Eq. (2.4) for $M = -4.035$ MeV, $K = 250$ MeV, and $\rho_0 = 0.160$ fm^{-3}.

TABLE II. Binding energy per nucleon for 32 nuclei for type I energy functional. The experimental values are from Ref. [48]. All numbers are in MeV.

Nuclei	$K =$ 200 MeV	$K =$ 250 MeV	$K =$ 300 MeV	Experiment
^{10}B	5.797	5.830	5.868	6.475
^{11}C	6.373	6.397	6.422	6.676
^{12}C	7.429	7.441	7.452	7.680
^{15}O	7.103	7.117	7.132	7.464
^{16}O	7.774	7.782	7.789	7.976
^{20}Ne	8.031	8.035	8.040	8.032
^{23}Na	8.071	8.076	8.083	8.111
^{27}Si	8.052	8.055	8.059	8.124
^{28}Si	8.353	8.353	8.355	8.448
^{31}S	8.197	8.198	8.201	8.282
^{32}S	8.450	8.449	8.450	8.493
^{39}Ca	8.372	8.370	8.371	8.369
^{40}Ca	8.564	8.561	8.560	8.551
^{44}Ca	8.742	8.741	8.742	8.658
^{48}Ca	8.571	8.575	8.580	8.666
^{50}V	8.711	8.710	8.711	8.696
^{51}V	8.754	8.753	8.754	8.742
^{58}Ni	8.739	8.734	8.731	8.732
^{88}Y	8.724	8.720	8.718	8.683
^{89}Y	8.734	8.731	8.730	8.714
^{100}Mo	8.654	8.654	8.654	8.605
^{122}Sn	8.491	8.491	8.492	8.488
^{138}La	8.381	8.380	8.380	8.375
^{139}La	8.383	8.373	8.373	8.378
^{150}Nd	8.267	8.267	8.289	8.250
^{169}Tm	8.146	8.145	8.143	8.115
^{174}Yb	8.101	8.101	8.101	8.084
^{198}Hg	7.915	7.913	7.911	7.912
^{207}Pb	7.831	7.831	7.831	7.870
^{208}Pb	7.823	7.823	7.824	7.867
^{238}U	7.579	7.581	7.582	7.570
^{243}Am	7.546	7.546	7.546	7.530

TABLE III. The experimental rms radii are taken from Ref. [47], error bars in square brackets and [46], error bar in parenthesis. The theoretical point rms radii are folded with the proton form factor. All rms radii are in fm. Calculations are for type I energy functional.

Nuclei	$K =$ 200 MeV	$K =$ 250 MeV	$K =$ 300 MeV	Experiment
^{10}B	2.414	2.425	2.435	2.450(120)
^{11}C	2.467	2.477	2.486	–
^{12}C	2.513	2.522	2.530	2.472(15)
^{15}O	2.649	2.655	2.661	–
^{16}O	2.688	2.694	2.699	2.728(8)
^{20}Ne	2.839	2.843	2.846	2.992(8)
^{23}Na	2.939	2.942	2.944	2.986 [9]
^{27}Si	3.068	3.069	3.071	–
^{28}Si	3.094	3.097	3.098	3.086(18)
^{31}S	3.182	3.183	3.183	–
^{32}S	3.208	3.208	3.208	3.239(30)
^{39}Ca	3.388	3.387	3.386	–
^{40}Ca	3.410	3.409	3.407	3.485 [3]
^{44}Ca	3.496	3.494	3.492	3.523 [5]
^{48}Ca	3.577	3.575	3.572	3.484 [5]
^{50}V	3.626	3.622	3.619	–
^{51}V	3.645	3.641	3.639	3.615(31)
^{58}Ni	3.789	3.784	3.780	3.783 [4]
^{88}Y	4.279	4.272	4.265	–
^{89}Y	4.293	4.285	4.278	4.240(20)
^{100}Mo	4.443	4.434	4.427	4.443 [4]
^{122}Sn	4.721	4.710	4.702	4.663 [1]
^{138}La	4.908	4.896	4.886	4.853 [8]
^{139}La	4.918	4.906	4.896	4.861 [8]
^{150}Nd	5.033	5.021	5.011	5.015(37)
^{169}Tm	5.233	5.218	5.206	5.226 [4]
^{174}Yb	5.279	5.264	5.252	5.312 [42]
^{198}Hg	5.505	5.488	5.474	5.441 [2]
^{207}Pb	5.580	5.563	5.549	5.504 [2]
^{208}Pb	5.587	5.571	5.557	5.505 [2]
^{238}U	5.834	5.815	5.800	5.859 [4]
^{243}Am	5.877	5.858	5.842	5.905 [4]

Since we consider values of K much outside the range of K of these interactions we have allowed M to vary freely in the fitting procedure.

For $K = 100$ and 400 MeV, the values of M are much too large. However the χ^2 values for K between 200 and 400 MeV vary only slightly. It is clear that compression modulus is quite insensitive, as also observed in earlier studies, to the static properties of nuclei.

The binding energies and rms radii are quite insensitive to the value of ρ_x. Thus at $K = 250$ MeV, changing ρ_x from 0.12 to 0.03 the χ^2 decreases only by 3%, whereas, in this range, the value of M increases by 83%. The only parameter which is sensitive to K and ρ_x is M. For a given ρ_x the relationship between K and M is quite linear. Other parameters are seen to vary very slowly but systematically, except a_ρ at $\rho_x = 0.09$ and $K = 100$ MeV.

The binding energies per nucleon (BE/nucleon) are shown in Table II for $K = 200, 250$, and 300 MeV. It is seen that BE/nucleon increases as K increases, though insignificantly, up to ^{31}S followed by a transition region which extends till ^{50}V and then it decreases as a function of K, again insignificantly, ultimately leveling off in the high mass number region. The same trend is obtained in case of rms radii as seen from Tables III, however, in this case no leveling off takes place in the high mass number region. In case of Hartree-Fock calculations with phenomenological effective interactions no such systematic trend have been observed as a function of K [25,26]. Further the differences in BE/nucleon and charge rms radii for different K are larger sometime by one order of magnitude compared to the results shown in Tables II and III. The reason for this discrepancy can be attributed to the consequence of having different ρ_0 and u_v for different values of K in the effective interactions displayed in Table IV, and also because they belong to different families or types of the interactions. The values of K, ρ_0 and u_v are taken from [25]. The values of K span a region of 193 to 356 MeV with ρ_0 changing from 0.206 to 0.145 fm^{-3}, which is typically a characteristic of such interactions. The interaction $B1$ is that of Brink and Boeker with a zero range spin-orbit force [49],

TABLE IV. The parameter values for various fits to binding energies and rms radii for type II energy functional. Note the very large values of χ^2 for $B1'$. For details, see text.

Interaction	ρ_0	u_v	K	ρ_x	a_ρ MeV	$a_{\rm sym}$ MeV	$a_{\rm pair}$ MeV	χ^2
B1′	0.206	15.70	193	0.12	33.049	20.571	63.515	56.04
				0.09	35.054	20.703	61.057	54.86
				0.06	36.786	20.880	57.661	53.82
				0.03	38.236	21.041	54.110	53.11
D1′	0.168	16.30	228	0.12	41.278	27.028	50.309	0.852
				0.09	43.308	27.233	47.688	0.714
				0.06	44.965	27.394	45.124	0.698
				0.03	46.162	27.509	42.768	0.749
Sk'_a	0.155	16.00	263	0.12	38.380	26.037	42.435	0.736
				0.09	39.754	26.158	41.125	0.717
				0.06	40.691	26.225	39.864	0.727
				0.03	41.187	26.263	39.306	0.740
SIV′	0.152	15.98	325	0.12	34.784	25.676	44.823	1.004
				0.09	35.161	25.694	44.629	0.968
				0.06	35.156	25.703	44.570	0.968
				0.03	34.759	25.696	44.906	1.008
SIII′	0.145	15.87	356	0.12	38.570	29.455	48.906	1.274
				0.09	39.523	29.374	50.988	1.271
				0.06	39.463	29.535	49.543	1.280
				0.03	39.786	29.470	50.414	1.292

D1 of Gogny [50], Sk_a of Köhler [51], and the Skyrme forces SIV and SIII of Orsay group [36]. In order to emulate these interactions in our formalism, at least partially, we use the values of K, ρ_0 and u_v from Table IV and obtain a fit to the static properties of nuclei following the procedure outlined earlier for all 32 nuclei. Since these effective interactions [26] do not contain large anharmonicity we restrict the value of M at -4 MeV. This restriction, though guided by the curve (d) in Fig. 1 is somewhat ad hoc; we believe it is representative of the interactions we are aiming to emulate. To distinguish the original interactions with the emulated interactions we denote them with a prime in the table. The values of the parameters and χ^2 are given in Table IV. To distinguish the two calculations, we name them as type I (Table I) and type II (Table IV) energy functional calculations. In Tables V and VI, we give the binding energies and rms radii for type II energy functional.

A qualitative and startling difference between the results of the two calculations is found in the values of K_A, the effective compression modulus. Using Eqs. (2.8) to (2.14) we plot in Figs. 2(a)–2(c), K_A as a function of K for all the 32 nuclei for type I functional and for ^{122}Sn (dashed curve) and ^{208}Pb (solid curve) for type II functional for different modes of compression or dilation of the nucleus [44]. These calculations are performed by assuming

$$\frac{\delta R}{R} = \alpha \frac{\delta t}{t} \tag{2.16}$$

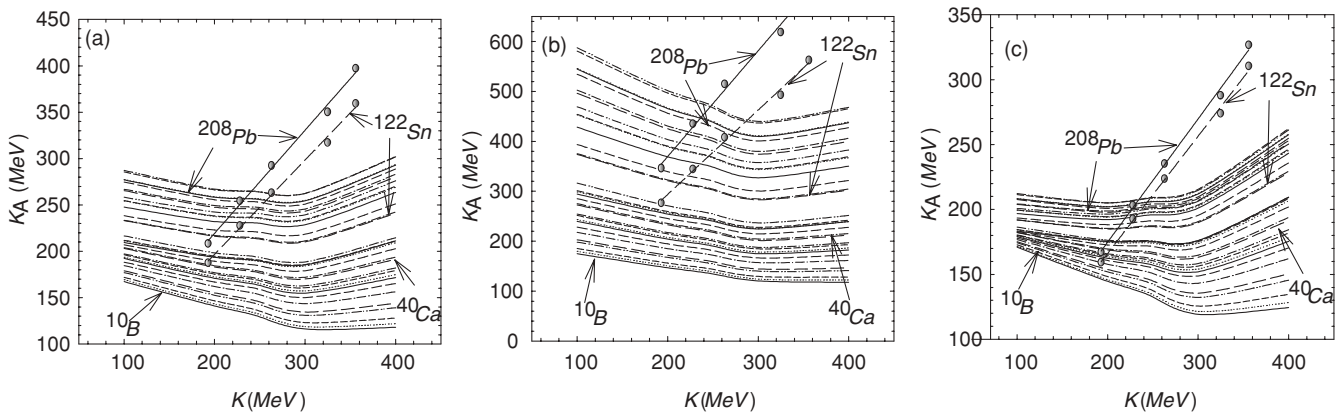

FIG. 2. The effective compression modulus K_A as a function of K for all the 32 nuclei for $\alpha = 1$ (a), $\alpha = 1/3$ (b), and $\alpha = 2.0$ (c). The filled and open circles are the values of K_A as a function of K for ^{208}Pb and ^{122}Sn computed by partially mimicking the various effective interactions (see text for details). The lines represent the best fit.

TABLE V. Same as in Table II. Calculations are for type II energy functional.

Nuclei	$K =$ 228 MeV	$K =$ 263 MeV	$K =$ 356 MeV	Experiment
^{10}B	5.643	5.752	5.340	6.475
^{11}C	6.295	6.344	6.101	6.676
^{12}C	7.426	7.418	7.349	7.680
^{15}O	7.035	7.084	6.916	7.464
^{16}O	7.753	7.766	7.702	7.976
^{20}Ne	8.007	8.025	7.702	8.032
^{23}Na	8.024	8.062	7.973	8.111
^{27}Si	8.016	8.047	7.981	8.124
^{28}Si	8.335	8.351	8.324	8.448
^{31}S	8.197	8.194	8.147	8.282
^{32}S	8.437	8.449	8.433	8.493
^{39}Ca	8.359	8.372	8.355	8.369
^{40}Ca	8.561	8.566	8.569	8.551
^{44}Ca	8.731	8.741	8.726	8.658
^{48}Ca	8.533	8.562	8.491	8.666
^{50}V	8.699	8.710	8.691	8.696
^{51}V	8.743	8.753	8.736	8.742
^{58}Ni	8.753	8.744	8.777	8.732
^{88}Y	8.736	8.727	8.750	8.683
^{89}Y	8.746	8.714	8.757	8.714
^{100}Mo	8.658	8.605	8.653	8.605
^{122}Sn	8.492	8.489	8.482	8.488
^{138}La	8.388	8.375	8.390	8.375
^{139}La	8.378	8.373	8.376	8.378
^{150}Nd	8.263	8.263	8.249	8.250
^{169}Tm	8.156	8.148	8.164	8.115
^{174}Yb	8.106	8.102	8.106	8.084
^{198}Hg	7.924	7.917	7.937	7.912
^{207}Pb	7.832	7.831	7.833	7.870
^{208}Pb	7.822	7.823	7.820	7.867
^{238}U	7.571	7.578	7.563	7.570
^{243}Am	7.543	7.546	7.546	7.530

TABLE VI. Same as in Table III. Calculations are for type II energy functional.

Nuclei	$K =$ 228 MeV	$K =$ 263 MeV	$K =$ 356 MeV	Experiment
^{10}B	2.455	2.408	2.376	2.450(120)
^{11}C	2.506	2.462	2.430	–
^{12}C	2.550	2.508	2.480	2.472(15)
^{15}O	2.680	2.644	2.620	–
^{16}O	2.717	2.684	2.662	2.728(8)
^{20}Ne	2.862	2.836	2.819	2.992(8)
^{23}Na	2.968	2.937	2.924	2.986 [9]
^{27}Si	3.083	3.067	3.057	–
^{28}Si	3.109	3.095	3.086	3.086(18)
^{31}S	3.193	3.182	3.176	–
^{32}S	3.218	3.208	3.203	3.239(30)
^{39}Ca	3.393	3.390	3.389	–
^{40}Ca	3.414	3.412	3.413	3.485 [3]
^{44}Ca	3.496	3.499	3.504	3.523 [5]
^{48}Ca	3.574	3.581	3.590	3.484 [5]
^{50}V	3.622	3.630	3.637	–
^{51}V	3.640	3.649	3.658	3.615(31)
^{58}Ni	3.781	3.793	3.804	3.783 [4]
^{88}Y	4.257	4.288	4.311	–
^{89}Y	4.270	4.301	4.325	4.240(20)
^{100}Mo	4.416	4.423	4.481	4.443 [4]
^{122}Sn	4.687	4.732	4.766	4.663 [1]
^{138}La	4.870	4.920	4.957	4.853 [8]
^{139}La	4.879	4.930	4.967	4.861 [8]
^{150}Nd	4.992	5.047	5.086	5.015(37)
^{169}Tm	5.186	5.246	5.287	5.226 [4]
^{174}Yb	5.231	5.292	5.335	5.312 [42]
^{198}Hg	5.452	5.518	5.563	5.441 [2]
^{207}Pb	5.525	5.594	5.641	5.504 [2]
^{208}Pb	5.533	5.602	5.649	5.505 [2]
^{238}U	5.773	5.849	5.899	5.859 [4]
^{243}Am	5.816	5.891	5.942	5.905 [4]

for different values of α. Here R, δR, t, and δt are the averages over neutrons and protons. $\alpha = 1$ gives equal emphasis to R and t in the scaling of the density, Fig. 2(a). Figure 2(b), $\alpha = 1/3$, corresponds to situation where by and large only the surface is participating in the compression or dilation of the nucleus, and $\alpha = 2$, Fig. 2(c), corresponds to vibrations more in the bulk region. In all three figures it is seen that there are large regions where K_A is much less sensitive to K for type I functional as compared to type II functional. It slowly decreases with increasing K and then increases gradually for large K. For type II functional, the solid curves for ^{208}Pb follow the same trend as found in earlier Hartree-Fock calculations with the effective interactions [26] mentioned earlier. Quite contrary to type I curves, here we see that K_A has a strong dependence and increases linearly with K. The two situations have implications not only on the polarizing effect of the Λ on core nuclei, but possibly also on the extraction of K from the giant monopole resonance energies [25,26,42]. The implication for the monopole resonances requires a separate study and is clearly outside the scope of the present work. Nonetheless, we would like to understand a little more on such diverse behavior of K_A as function of K. We find that it is related in a crucial way with the properties of nuclear surface. We examine this briefly in what follows now.

In Fig. 3 we plot $\varepsilon(\rho)$ as function of ρ for K between 200 and 300 MeV for type I functional. It is seen that the values of $\varepsilon(\rho)$ change their trends for $\rho < 0.07$ fm^{-3}. For example, at lower densities $\varepsilon(\rho)$ for $K = 200$ becomes larger compared to other values of K. This occurs because M dominates at lower densities. Our $\varepsilon(\rho)$ for $K = 250$ MeV is also plotted in Fig. 1 to compare it with the $\varepsilon(\rho)$ of Argonne AV$_{18}$+UIX [38,39,41] $\varepsilon(\rho)$. It is useful to define a local compression modulus for any value of ρ, $K_l = 9\rho^2 d^2\varepsilon(\rho)d\rho^2$. In Fig. 4, K_l is plotted as function of ρ. It is seen that for $K = 200$ MeV, K_l increases as ρ decreases from $\rho = 0.2$ fm^{-3}. On the other hand for $K = 300$ MeV there is a rapid drop all along the values of ρ as it decreases. Thus, in nuclei the surface contribution of K_l compensates for the bulk modulus of the bulk or the interior region in order to fit the static properties of nuclei. This then leads to an almost constant K_A as shown in Figs. 2(a)–2(c) in certain regions and weak dependence in other regions.

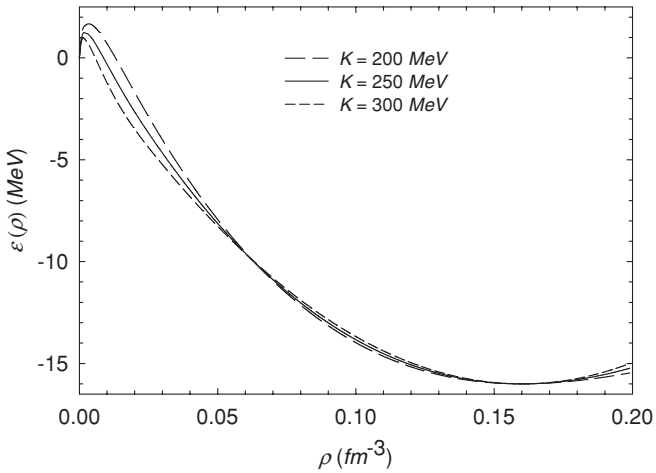

FIG. 3. The curves represent the equation of state of symmetric nuclear matter as a function of density ρ for various K.

For the present study our results for both the types of energy functional are quite reasonable as we are interested in the differences of ${}^{A-1}E$ and ${}^{A-1}\hat{E}$, and in changes of the rms radii in the presence of Λ. This is evident from Tables I to VI. The only exception being BI' which has very large values of χ^2. It is well known that the interaction of Brink and Boeker [49] does not give a good account of the binding energies and rms radii [25].

It is not difficult to envisage that with further corrections of shell effects, deformation, pairing correlations and an added density dependent term in the asymmetry energy, our approach may compete with other modern mass formulae which use Skyrme density functional [52,53].

III. HYPERNUCLEI

The total hypernuclear energy of Eq. (1.1) requires the calculation of $E_\Lambda[\rho]$. This may be calculated either by a phenomenological approach such as that of Millener *et al.* [54] or, as in the present work, by a more microscopic approach using a local density approximation. For this purpose, we make use of semirealistic ΛN plus dispersive and two-pion exchange ΛNN interactions which are generally consistent with meson theoretic models and which satisfactorily describe the s-shell hypernuclei binding energies and low energy Λp scattering data. Though, these calculations have been performed earlier [3,7,8], but we carry them out here in a more consistent manner, i.e., s-shell hypernuclei and Λ-binding to nuclear matter $D(\rho)$ are calculated using the same level of approximation. We thus neglect the three-body correlations in s-shell hypernuclei since technique for incorporating these in nuclear matter is not yet developed. The calculations for heavier hypernuclei and core polarization effects are described in Sec. (III B). For the nucleonic part of the Hamiltonian we use the AV_{18} + UIX interaction [38] for the s-shell hypernuclei and use the model of the previous section for heavier hypernuclei.

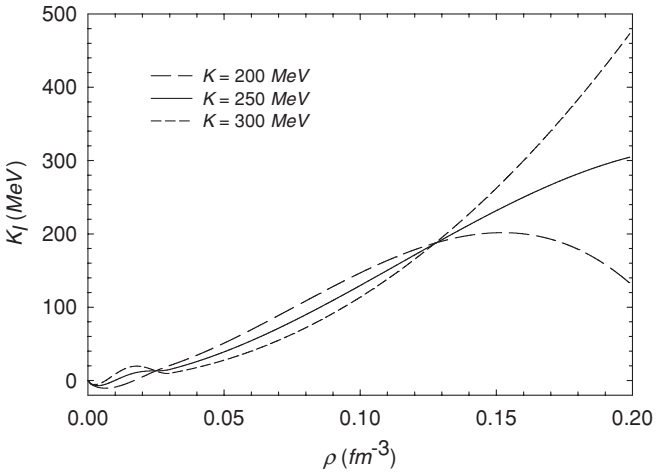

FIG. 4. K_l as a function of ρ for various values of K.

A. Λp scattering, s-shell hypernuclei and Λ-binding in nuclear matter

For the ΛN interaction, we use

$$V_{\Lambda N} = \left[V_c(r) - \bar{V}T_\pi^2(r)\right](1 - \varepsilon + \varepsilon P_x) + \tfrac{1}{4}V_\sigma T_\pi^2(r)\vec{\sigma}_\Lambda \cdot \vec{\sigma}_N, \tag{3.1}$$

where P_x is Majorana space-exchange operator and ε is the corresponding exchange parameter. $V_c(r)$ is a Woods-Saxon core which generates a repulsion of more than 2000 MeV at the center $\bar{V}$ and V_σ are respectively the spin-average and spin dependent strengths, and T_π is a one-pion tensor shape factor with cutoff. The parameters of our interaction are constrained to fit the low energy Λp scattering including the F/B ratio [56]. This determine $\bar{V}$ and ε. We use $\bar{V} = 6.15$ MeV and $\varepsilon = 0.29$ which also has a bearing to Λ single particle energies [9]. The value of ε is somewhat higher than employed in Refs. [7,8,57], but is consistent with the F/B ratio. V_σ is essentially fixed by the energy splitting of the mass 4 hypernuclear system, however it is correlated with the spin dependence of three-body ΛNN interaction. We use a value of $V_\sigma = 0.176$ as found in [8].

The $V_{\Lambda NN}$ interaction consists of a two-pion exchange and a dispersive part:

$$V_{\Lambda NN} = V_{\Lambda NN}^{2\pi} + V_{\Lambda NN}^{\mathrm{DS}}, \tag{3.2}$$

$$V_{\Lambda NN}^{2\pi} = -\tfrac{1}{6}C_p\vec{\tau}_{N_1} \cdot \vec{\tau}_{N_2}\left\{X_{N_1\Lambda}, X_{N_2\Lambda}\right\}, \tag{3.3}$$

$$V_{\Lambda NN}^{\mathrm{DS}} = W_o \sum_{cycl} T_\pi^2(r_{N_1\Lambda})T_\pi^2(r_{N_2\Lambda})\left[1 + \tfrac{1}{6}\vec{\sigma}_\Lambda \cdot (\vec{\sigma}_1 + \vec{\sigma}_2)\right]. \tag{3.4}$$

The curly bracket in Eq. (3.3) represents the anticommutator and the factors $X_{N\Lambda}$ are given by

$$X_{N\Lambda} = T_\pi(r_{N\Lambda})S_{N\Lambda} + Y_\pi(r_{N\Lambda})(\vec{\sigma}_\Lambda \cdot \vec{\sigma}_\Lambda),$$

where Y_π is the radial function associated with the Yukawa part of the one-pion exchange potential with a cut off and $S_{N\Lambda}$ is the usual tensor term. $V_{\Lambda NN}$ arise mainly from the elimination of Σ degrees of freedom and is found essential for a consistent phenomenology of s-shell hypernuclei, when use is made of $V_{\Lambda N}$ which accounts for low energy Λp scattering data. We use the following values for the $V_{\Lambda NN}$ interaction

TABLE VII. Comparison of calculated and experimental binding energies of s-shell hypernuclei. Rows two and three give the average values of ${}^{4}_{\Lambda}$H and ${}^{4}_{\Lambda}$He.

Hypernucleus	Calculated B_Λ in MeV	Experiment B_Λ in MeV
${}^{3}_{\Lambda}$H	0.24 ± 0.03	0.13 ± 0.05
${}^{4}_{\Lambda}$H, ${}^{4}_{\Lambda}$He	1.66 ± 0.05	2.22 ± 0.04
${}^{4}_{\Lambda}$H*, ${}^{4}_{\Lambda}$He*	0.93 ± 0.06	1.12 ± 0.06
${}^{5}_{\Lambda}$He	3.27 ± 0.10	3.12 ± 0.02

parameters:

$$C_p = 2.0\,\text{MeV} \quad \text{and} \quad W_o = 0.01\,\text{MeV}. \tag{3.5}$$

The above values of the parameters then give, to some extent, a reasonable account of s-shell hypernuclear binding energies, Table VII. The mass 3 system is overbound and the ground state of the mass 4 system is underboud. This is probably the price one has to pay for the consistency (without the three-body correlations) with the nuclear matter calculations which are more important to the present study.

B. Calculation of E_Λ and core polarization

The details of the calculations of E_Λ for a given core nucleus density distribution are described in Refs. [9,27,28] where it was shown that the s.p. data can be well described using ΛN plus dispersive ΛNN and two-pion exchange ΛNN forces. We briefly outline this procedure. We use a variational wave function to calculate the Λ-binding to nuclear matter, $D(\rho, k_\Lambda)$ at a density ρ and for a Λ momentum k_Λ. The various expectation values are calculated using the Fermi hypernetted chain (FHNC) approximation (for details see Refs. [9,55]). The single particle potential felt by Λ inside a nucleus is then approximated as

$$U_\Lambda^{A-1}(r) = D(\rho^{A-1}, k_\Lambda = 0) \equiv D(\rho^{A-1}(r)), \tag{3.6}$$

where the density ρ^{A-1} of the core nuclei is obtained as a result of the minimization procedure described in Sec. II. In this respect, our calculation of E_Λ is different from that of Ref. [9], where the densities ρ^{A-1} were obtained from electron scattering data. The dependence of U_Λ^{A-1} on k_Λ, is simulated though an effective mass m^*_Λ which, in the present approach results from the exchange part of the ΛN force which arises from K, K^* exchange. $E_\Lambda(\rho^{A-1})$ for a given ℓ_Λ is then obtained from solution of the radial Schrödinger equation

$$\left[-\frac{\hbar}{2\mu^*_\lambda(\rho(r))}\frac{d^2}{dr^2} + \frac{\hbar^2\ell_\Lambda(\ell_{\Lambda+1})}{2\mu^*_\Lambda(\rho(r))r^2} + U_\Lambda^{A-1}(r)\right]\phi_{\ell_\Lambda} = E_\Lambda\phi_{\ell_\Lambda}. \tag{3.7}$$

The dependence of E_Λ on ρ^{A-1} arises through the dependence of U_Λ^{A-1} and of μ^*_Λ on ρ^{A-1}, where μ^*_Λ is the effective reduced mass of the effective mass of Λ and the mass of the core nucleus. This is given by

$$\frac{1}{\mu^*_\Lambda} = \frac{1}{M_{A-1}} + \frac{1}{m^*_\Lambda(\rho(r))}, \tag{3.8}$$

where M_{A-1} is the mass of the core-nucleus.

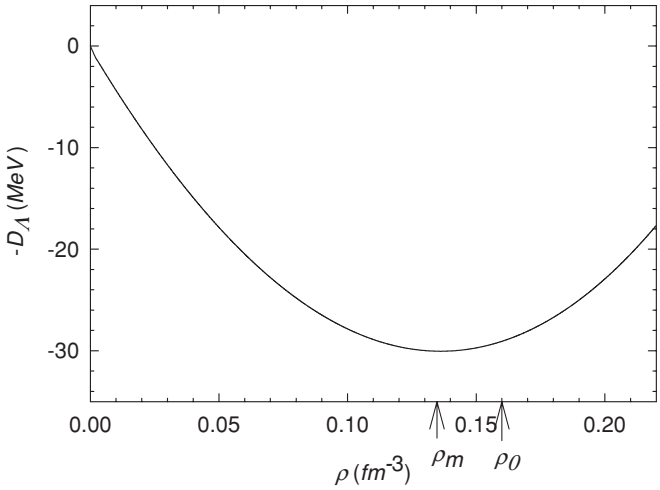

FIG. 5. The solid curve represents the Λ binding to nuclear matter $-D_\Lambda$.

$D(\rho)$ is shown in Fig. 5 and m^*_Λ/m_Λ as function of density is shown in Fig. 6. As argued in Refs. [9,27,28] $D(\rho)$ must have "saturation" properties in the sense that it should have a maximum ρ_m near ρ_0 in order to allow a satisfactory fit to the s.p. data. This observation has also been made by Millener *et al.* [54] in their purely phenomenological approach and also by Lombard *et al.* in their relativistic mean-field calculations [58]. Microscopically this maximum is due to the competition between the attractive contribution of direct ΛN force and the repulsive contributions of the ΛN exchange and the three-body ΛNN forces. To obtain the energy of the hypernucleus including core polarization we minimize

$${}^{A}_{\Lambda}E[\rho^{A-1}] = {}^{A}E[\rho^{A-1}] + E_\Lambda[\rho^{A-1}] \tag{3.9}$$

with respect to the parameters $R_{n(p)}$ and $t_{n(p)}$ of ρ^{A-1}. This gives a slightly changed core density $\hat\rho^{A-1}$ and the core energy ${}^{A-1}E[\hat\rho^{A-1}]$ due to the presence of the Λ. The results for the Λ s.p. are shown in Fig. 7 for $K = 250$ MeV for type I energy functional. The results for other values of K are not very different.

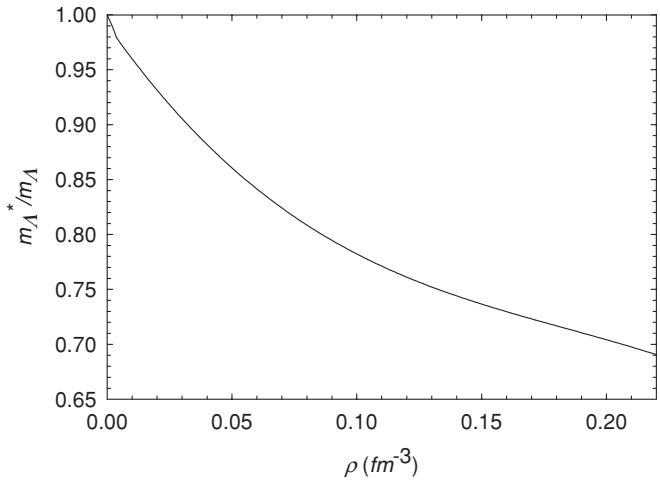

FIG. 6. The effective mass of Λ as a function of density ρ.

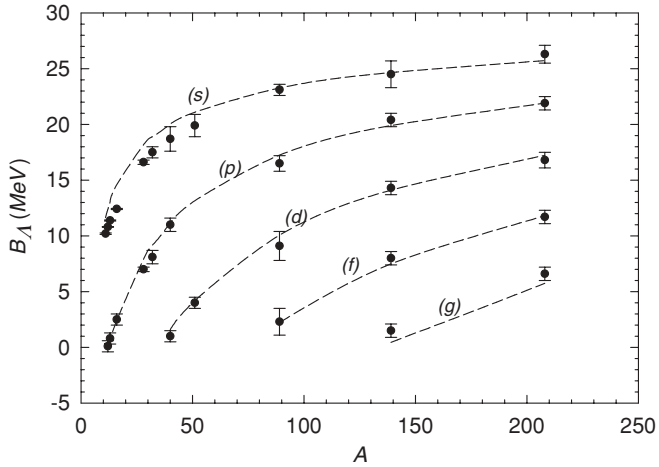

FIG. 7. Λ single particle energies (B_Λ) as a function of mass number for different angular momentum states. The experimental points are from Ref. [45]. The dashed curves represent the results of the calculation as explained in the text.

The core polarization energy is defined as

$$\Delta E = {}^{A-1}E[\hat{\rho}^{A-1}] - {}^{A-1}E[\rho^{A-1}]. \tag{3.10}$$

This is positive since the minimum of ${}^{A-1}E$ alone is obtained for ρ^{A-1}. The change in the rms is defined as

$$\Delta R = \langle r^2\rangle^{1/2}_{A-1} - \langle r^2\rangle^{1/2}_{A-1} \tag{3.11}$$

where r and $\hat{r}$ refer to the absence and presence of the Λ particle, respectively. ΔR will be positive or negative depending upon the contraction or expansion of the core nucleus.

IV. CORE POLARIZATION RESULTS AND DISCUSSION

Figures 8 and 9 show our results for the core polarization energy ΔE and the change in the core radius ΔR for $K =$ 200, 250, and 300 MeV for type I functional. These calculations are performed for $D(\rho)$ and Λ effective mass of Figs. 5 and 6, respectively. It is observed that both ΔE and ΔR are quite small. Since these quantities are differences of two large quantities great care was required in minimizing the energy. An accuracy of up to seven significant digits was needed in the energy calculations for heavy nuclei to arrive at a meaningful result. As a result there were small kinks in both the curves, i.e., for ΔE and ΔR. There is no reason for the appearance of the kinks, except due to the accuracy of the calculations, since we do not include shell effects and the pairing energy does not depend on the density. For presentation purposes we have smoothed out the kinks without sacrificing the contents and the physical effects represented by the curves. No such smoothing was needed in case of the linear behavior of $D(\rho)$ as a function of ρ. There, both ΔE and ΔR are much larger (see Figs. 10 and 11).

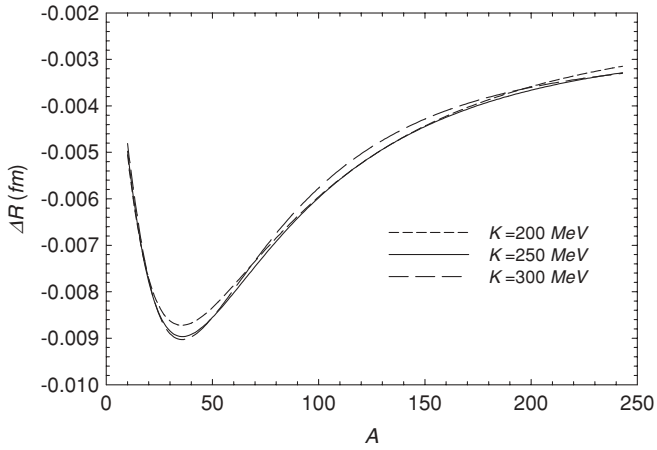

FIG. 9. Change in rms radii as a function of mass number for type I energy functional for various values of K.

It is seen in Fig. 9 that ΔR is negative for all the nuclei which correspond an outflow of nucleons from the interior to the surface. This is in contrast to a nonsaturating $D(\rho) = D_0\rho/\rho_0$ (with $D_0 = 30$ MeV = empirical well depth) where the proportionality to ρ arises microscopically from a direct nonexchange ΛN force. Such a $D(\rho)$, as is well known, favors

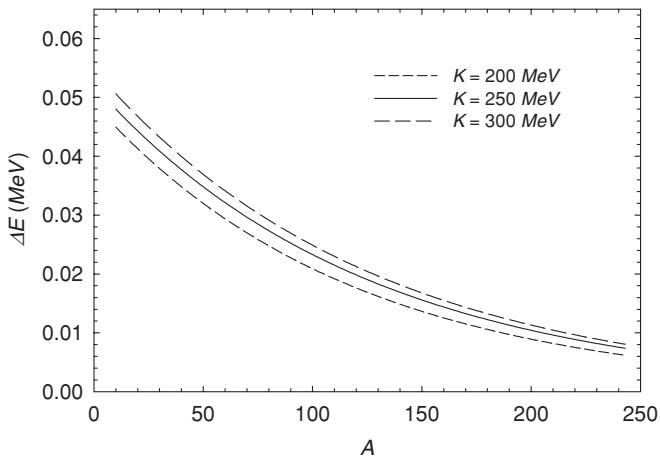

FIG. 8. Polarization Energy in MeV as a function of mass number for type I energy functional for various values of K.

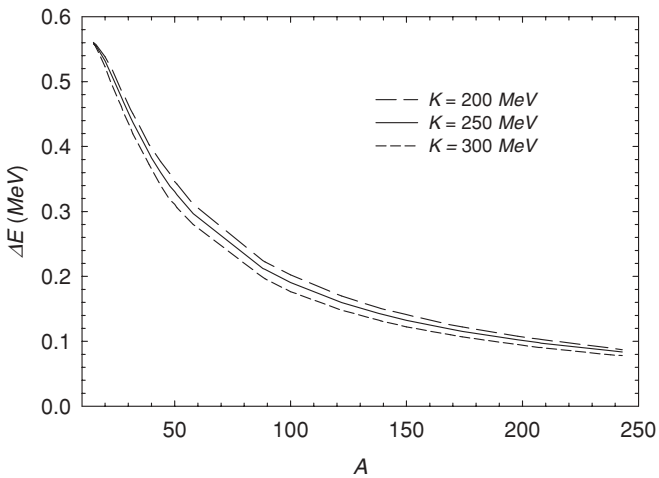

FIG. 10. Polarization energy in MeV as a function of mass number with $D_\Lambda = 30\rho/\rho_0$ for type I energy functional.

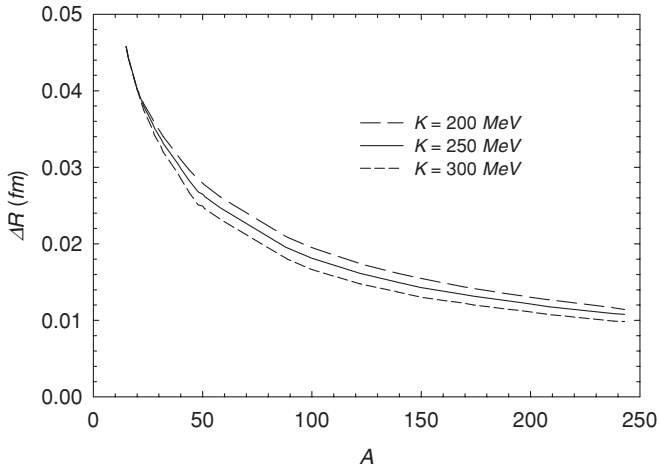

FIG. 11. Changes in rms radii as a function of mass number with $D_\Lambda = 30\rho/\rho_0$ for type I functional.

a contraction of the nucleus since the Λ binding will increase if ρ increases throughout the nucleus. On the other hand, for a "saturating" $D(\rho)$, with ρ_m fairly close to ρ_0 , changes of ρ in the nuclear interior are much more energy neutral for the Λ, whereas an increase of ρ in the surface increases the contribution of $D(\rho)$ to the Λ binding, thus favoring a flow of nucleons from the interior to the surface. The driving force tending to increase the Λ binding is thus expected to be smaller than for $D(\rho) \propto \rho$, and correspondingly both ΔE and $|\Delta R|$ are expected to be less. This is in fact the case as depicted for ΔE in Fig. 8 and for $|\Delta R|$ in Fig. 9, where $\Delta E \approx 0.03$ MeV and $|\Delta R| \approx 0.008$ fm around $A \approx 50$. It is important to note that the "driving force" of the Λ, giving the core polarization, is determined by the derivative of $D(\rho)$ with respect to ρ and not by its absolute value. The Λ exerts a deforming force in the sense that it tends to change the nuclear density to the value ρ_m [where $D(\rho)$ is maximum]. On the other hand, the nucleus tries to keep the density inside the nucleus near ρ_0, the equilibrium density. Thus there is trade off with the consequence that the density of the nucleus inside the nucleus decreases resulting in a net flow of matter from interior to exterior region. On the other hand in the surface region, where the density is less than ρ_0 the Λ particle will tend to increase the density resulting in a somewhat smaller surface thickness. For a nonsaturating $D(\rho) = 30\rho/\rho_0$, the Λ tries to increase the density of nucleus in all the regions causing a significant reduction in the rms radii. Also the core polarization energies will be much larger. In Figs. 10 and 11 we present our results for ΔE and ΔR for the non-saturating $D(\rho)$. Here, it is clearly seen that core polarization energies and changes in rms radii are one order of magnitude larger compared to saturating $D(\rho)$, and also ΔR is positive, demonstrating a contraction of the core nucleus.

We make the following observations from Figs. 8–11. These are (a) the dependence on K of the polarization energies and the rms radii is very weak, the curves as a function of K are very close to each other; (b) in Figs. 8 and 9, both, ΔE and ΔR values show an opposite trend as compared to found in earlier studies, i.e., they are found to be proportional to K instead of an inverse proportionality. This is seen in Fig. 8 rather clearly. Figure 9 shows a mixed trend, i.e., in some regions $K = 200$ and 300 MeV change trends, which can also be attributed to the accuracy of the calculations. However in Figs. 10 and 11, the trends as a function of K are opposite to that of Figs. 8 and 9, i.e., both ΔE and ΔR are proportional to K^{-1}. (c) In Fig. 9, the ΔR shows a distinct minimum around $A = 30$–40, and (d) for medium and large A nuclei both the quantities show an A^{-1} behavior.

The trends of the curves, as mentioned in the preceding paragraph, can be largely understood from the behavior of K_A, the effective compression modulus, as functions of K and A, and also from the saturating and nonsaturating character of $D(\rho)$ and a delicate balance among them. In fact, both ΔE and ΔR depend directly on K_A instead of K. However, this point needs further investigation and it would be desirable to establish it in a rigorous way. Though the present treatment is also rigorous but numerical in nature and thus confined to specific cases. For type I energy functional, K_A changes very little between $K = 100$ to 400 MeV and more so between 100 and 300 MeV [see Figs. 2(a)–2(c)]. This makes clear the clustering of curves for the three values of $K = 200$, 250, and 300 MeV as a function of A in all the four figures. Secondly as K increases K_A decreases very slowly. This means that overall core nucleus is "soft" for larger values of K thus giving somewhat greater values of ΔE and $|\Delta R|$ due to a relatively larger response of the core to the Λ. This explains the behavior of curves (Figs. 8 and 9) mentioned in (b) in the preceding paragraph. These curves correspond to the saturating $D(\rho)$ for which the Λ particle wave function is relatively pulled out to the surface region where the local compression modulus K_l are generally larger for smaller K (see Fig. 4 for the behavior of K_l as a function of ρ). In Fig. 12, we plot s-state Λ wave function $\phi_\Lambda(r)$ as a function of r for ^{40}Ca for $K = 200$ MeV, both for saturating and nonsaturating $D(\rho)$. It is seen that $\phi_\Lambda(r)$ is pulled out for the saturating $D(\rho)$ compared to the nonsaturating $D(\rho)$, despite the fact that it is more bound by ∼1.5 MeV. Thus for a nonsaturating $D(\rho)$, the Λ particle spends more time inside the core region of the nucleus. This, perhaps, explains the K^{-1} behavior of ΔE and ΔR in Figs. 10

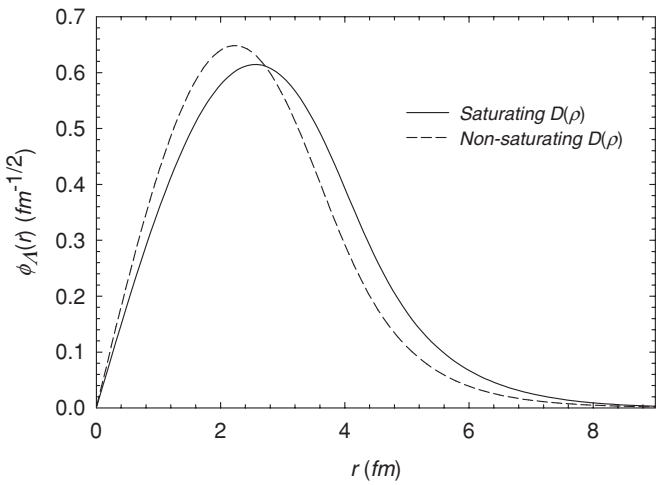

FIG. 12. The Λ wave function in s-state for saturating and nonsaturating $D(\rho)$ for type I functional.

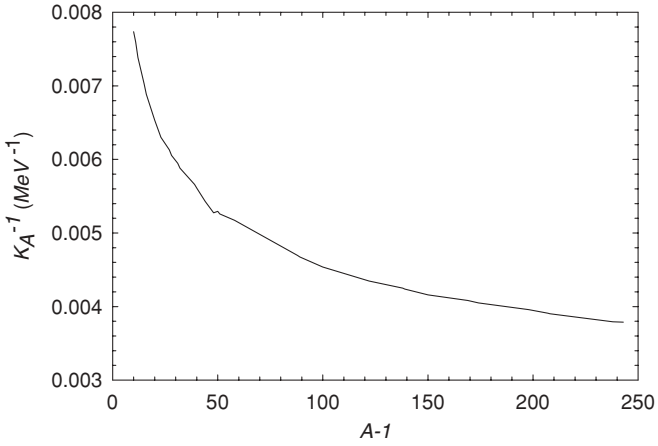

FIG. 13. The inverse of the effective compression modulus as a function of the mass number for $K = 250$ MeV.

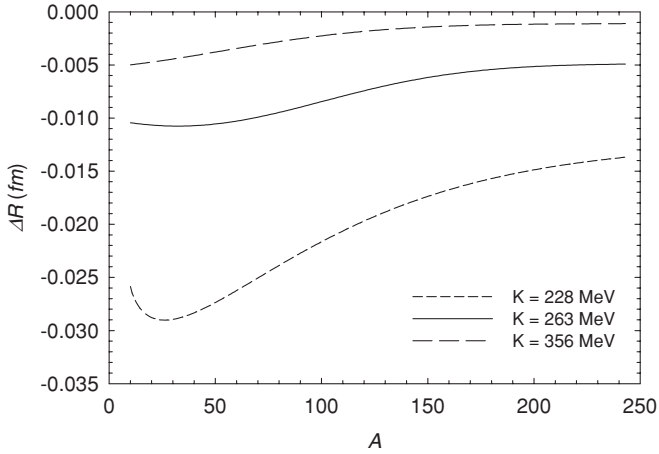

FIG. 15. Change in rms radii as a function of mass number for type II energy functional for various values of K.

and 11, but still the curves are clustered signifying a very weak dependence on K. The occurrence of minima in ΔR in Fig. 9 can be understood by realizing that light nuclei consist of large surface regions, compared to the core, where a considerable fraction of the densities have values less than ρ_m. Thus not having enough nucleons in the core region, the Λ may shrink the surface leading to a less expansion of the nucleus. In fact this phenomenon may also lead to contraction for A less than 10, as witnessed experimentally in ${}^{7}_{\Lambda}$Li [24] and in the theoretical studies of s-shell hypernuclei [8] where core radii in the s-shell region were found to shrink significantly. Finally, dependence of ΔE and $|\Delta R|$ on A can be understood as a result of the core polarization being roughly a "$1/A$" effect. One Λ forcing the core distortion versus A core nucleons responding. The relative importance of the nuclear core and the surface region plays an important role. This effect is contained in the values of K_A as seen from Figs. 2(a)–2(c). In Fig. 13, we plot K_A^{-1} as a function of mass number for $K = 250$ MeV. It is amazing to see that K_A^{-1} follows the same trend as ΔE and $|\Delta R|$ as a function of A. Nuclei with higher mass number are in general harder to deform compared to nuclei with lower mass number, since they have higher effective compression modulus. This is related to ratio of number of nucleons in the core and the surface region.

In Figs. 14 and 15, we give the results for ΔE and ΔR for type II energy functional. These correspond to the saturating $D(\rho)$ of Fig. 5. In Figs. 2(a)–2(c), we have seen that for type II energy functional K_A strongly depends on K and is directly proportional as revealed by the solid and dashed curves for ^{208}Pb and ^{122}Sn nuclei, respectively. This effect is reflected in Figs. 14 and 15 where the ΔE and ΔR curves are widely spaced for different values of K and their values are proportional to K^{-1} for a given A. In this case also both ΔE and $|\Delta R|$ are quite small as in Figs. 8 and 9. Results for nonsaturating $D(\rho)$ are one order of magnitude higher and their values are on expected lines in accord with previous studies [11–22]. These are given in Figs. 16 and 17.

We now refer the reader to [11] and [16], where it was found that in the Hartree-Fock calculations the core polarization energy increases with A or at least stays constant in the range $8 < A < 40$. How do we reconcile or explain this result in

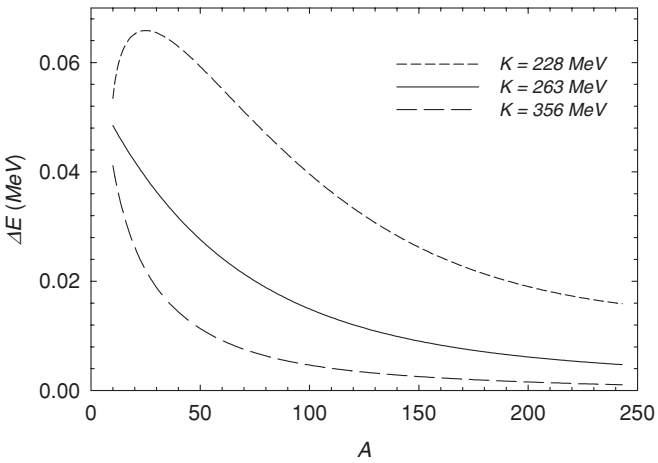

FIG. 14. Polarization energy in MeV as a function of mass number for type II energy functional for various values of K.

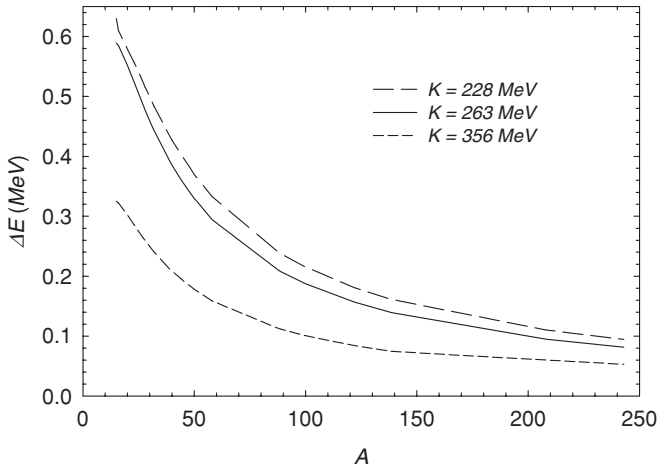

FIG. 16. Polarization energies as a function of mass number A for type II density functional with $D(\rho) = 30\rho/\rho_0$ for various values of K.

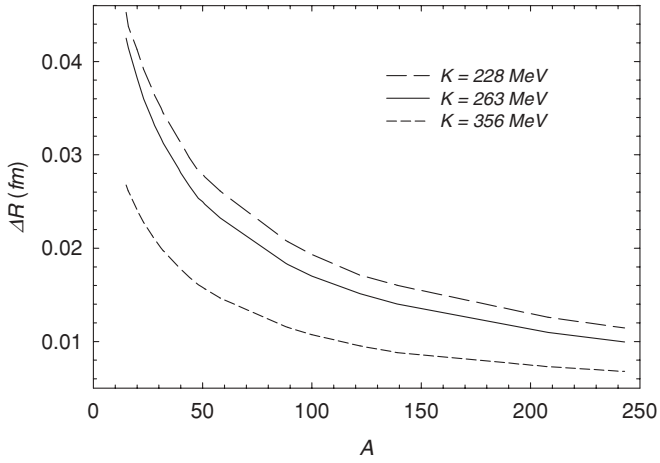

FIG. 17. Changes in rms radii as a function of mass number A for type II density functional with $D(\rho) = 30\rho/\rho_0$ for various values of K.

the context of the present work? We believe this is probably related to the values of K_A and/or to the characteristics of the equation of state and the associated values of K_l for the effective NN interaction employed in [11,16]. For example, in the Hartree-Fock calculations of the Saclay group [26] which use various effective interactions "... a 50% variation in A, say, from $A = 100$ to $A = 200$, induces only a variation of less than 5% in K_A." Does this provide a plausible answer in terms of the insensitivity of K_A as function of A (in the Hartree-Fock calculations) in combination with other factors? We have a somewhat similar situation as depicted in Figs. 14 and 15 for type II functional. Here we see that for $K =$ 228 MeV, ΔE first rises, reaches a peak and then decreases on expected lines for medium and large A. ΔR follows the same pattern. These possibly could also arise due to delicate balance of competing factors mentioned earlier.

We would like to offer some comments on types I and II functionals. The behavior of type I functional leads to circumstances similar to that encountered in condensates of cold atoms in a magnetic trap. It has been shown that, in certain frequency range, there is no connection between the frequencies of monopole vibrations of a finite quantum system (of a Bosonic condensate) with the compression modulus of the corresponding infinite matter [59,60]. An analogous situation is encountered here. The near independence of K_A from K implies that the core polarization energies and changes in rms radii due to presence of Λ are weakly dependent on K in the range 200 to 300 MeV. Thus, they are insensitive to the values of K as the binding energies and rms radii of nuclei are. In this respect the physics of nuclei with type I functional is similar to that of condensates in a magnetic trap. The situation with type II functional is quite different. Though, the binding energies and rms radii are more or less independent of K, but ΔE and ΔR depend sensitively on K. The present study cannot shed any light as to which type of functional correspond to reality. There is another interesting observation regarding our functionals; K_A is roughly proportional to A, Figs. 2(a)–2(c), more so for type I functional. Thus lighter nuclei are "softer" to deform compared to heavier nuclei. This is probably related

TABLE VIII. Results for a few ΛΛ-hypernuclei demonstrating the core polarization effects.

Hypernuclei	Saturating $D(\rho)$		Nonsaturating $D(\rho)$	
	ΔE (MeV)	ΔR (fm)	ΔE (MeV)	ΔR (fm)
${}^{18}_{\Lambda\Lambda}O$	0.142	−0.0127	2.340	0.0846
${}^{42}_{\Lambda\Lambda}$Ca	0.131	−0.0158	1.575	0.0587
${}^{91}_{\Lambda\Lambda}Y$	0.088	−0.0123	0.850	0.0386
${}^{210}_{\Lambda\Lambda}Pb$	0.037	−0.0072	0.390	0.0234

to some function of the ratio of number of nucleons in the surface to core region. It is not an "1/A" effect in the usual sense, like the center of mass correction in the calculation of energies with translationally noninvariant wave functions.

We would like to emphasize that our conclusion $\rho_m < \rho_0$ is not based upon the Λ s.p. data alone. In the framework of the present study, a consistent account of s-shell hypernuclei, Λp scattering, $D(\rho_0)$ along with Λ s.p. data, requires $\rho_m < \rho_0$. We do not establish it as an absolute law.

For illustrative purposes we also give in Table VIII a few results for ΛΛ-hypernuclei neglecting ΛΛ interaction, both for saturating as well as nonsaturating $D(\rho)$. It is seen that the effect of polarization enhances by a factor of 3 to 4 compared to single Λ-hypernuclei, however, the effect with the saturating $D(\rho)$ is still small. Also, as in single Λ-hypernuclei, the effect with the nonsaturating $D(\rho)$ is one order of magnitude larger. In Fig. 18 we plot the densities of ^{40}Ca with and without the two Λs. It demonstrates the flow of nuclear matter from the interior to the surface region. In a later publication, we shall take up the hypernuclei ${}^{6}_{\Lambda\Lambda}$He in a fully variational framework and ${}^{13}_{\Lambda\Lambda}$B in the present framework using realistic ΛΛ and other interactions.

Lastly, we comment on an inconsequential minor inconsistency in the context of the present work. This results by assuming that $a_{\rm sym}$ is independent of ρ. Information on the ρ

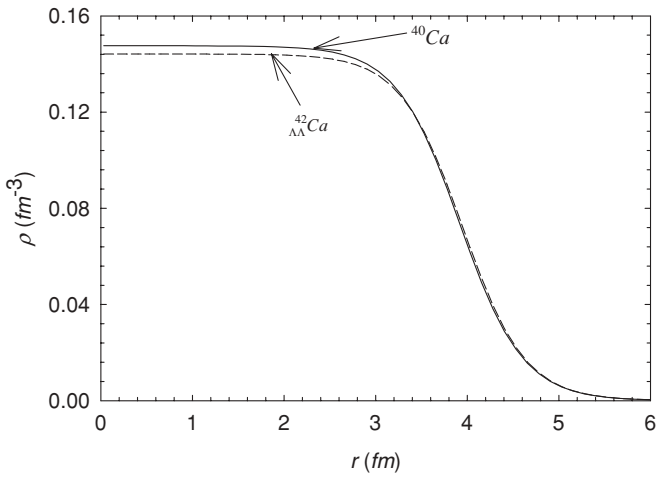

FIG. 18. The nucleon single particle densities for the nucleus ^{40}Ca (solid line) and the hypernucleus ${}^{42}_{\Lambda\Lambda}$Ca (dashed line). It may be seen that the presence of Λs causes flow of matter from the interior to the exterior region.

dependence of $a_{\rm sym}$ requires additional experimental data, in particular accurate measurement of rms radii of the neutron distributions. As shown in [61] the difference between $\rho_n(r)$ and $\rho_p(r)$ is quite small for any reasonable assumption about the ρ dependence of $a_{\rm sym}$ and can be neglected for the purposes of this paper. Assuming the neutron and proton distributions to be the same, i.e. $\rho_p(r) = (N/A)\,\rho(r)$, $\rho_p(r) = (Z/A)\rho(r)$ is consistent with assuming $a_{\rm sym}$ to be independent of ρ and also neglecting the effect of coulomb forces on $\rho_p(r)$ and thus on the difference between $\rho_n(r)$ and $\rho_p(r)$. By themselves, the coulomb forces give a slightly more extended $\rho_p(r)$ than $\rho_n(r)$ in the surface region. In the tail region we find that the neutron density dominates as the proton distribution is slightly sharper than neutron distribution. With $a_{\rm sym}$ independent of ρ and $\rho_n(r) = \rho_p(r)$, the asymmetry energy is then just $a_{\rm sym}(N-Z)^2/A$. Calculations with these modifications were also carried out for a few test cases. No significant changes were found in the results. In fact, our calculation for K_A, (2.16), follow this procedure where we take an average of the neutron and proton densities.

V. CONCLUSIONS

We have developed a variational local density theory to calculate the changes that a Λ particle induces in nuclei. The theory is severely constrained by the Λ-single particle data, s-shell hypernuclei binding energies, low energy Λp scattering and the nuclear binding energies and rms radii. Our main conclusions are as follows:

(i) It is demonstrated that the effective compression modulus, K_A usually employed in the calculations of breathing modes of nuclei has a direct bearings on the core polarization effects. It may have very weak (with slight decrease with K), totally independent or strong dependence with direct proportionality to K depending upon the type of energy density functionals employed in the calculation.

(ii) Overall, the core polarization energies are quite small; this in turn justifies a large number of calculations on Λ-hypernuclei where core polarization energies have been completely neglected. This also lends support that Λ-hpernuclei constitute a simple system where the single particle picture is valid to a good approximation.

(iii) Though the Λ interacts strongly with the core nucleus, it induces only a small change due to the "saturation" properties of $D(\rho)$. From this aspect, the Λ may be considered as a weakly interacting probe. To exploit this situation and make progress in this direction, we have to wait for new developments in the field, both experimental as well as theoretical.

(iv) There are strong indications that the Λ causes a flow of nuclear matter from the interior to the exterior regions in nuclei. This may have interesting consequences for hypernuclei with several Λ's.

(v) The theory developed here can be easily extended to multi-Λ-hypernuclei. However, we have to include multi-Λ correlations within a variational framework if realistic $\Lambda\Lambda$ interactions are employed.

ACKNOWLEDGMENTS

Q.N.U. is grateful to Drs. D. J. Millener (BNL), Jean-Paul Blaizot (Saclay), D. E. Lanskoy (MSU), and S. Shlomo (Texas A & M) for correspondence. He is also grateful to Professor Richard F. Casten for allowing him to use the computing facilities of the Wright Nuclear Structure Laboratory at Yale University for part of this work and to John Baris for help in computing.

[1] R. H. Dalitz, R. C. Herndon, and Y. C. Tang, Nucl. Phys. **B47**, 109 (1972).
[2] A. Gal, Adv. Nucl. Phys. **8**, 1 (1975) and references therein.
[3] A. R. Bodmer and Q. N. Usmani, Nucl. Phys. **A477**, 621 (1988).
[4] A. R. Bodmer, Q. N. Usmani, and J. Carlson, Phys. Rev. C **29**, 684 (1984).
[5] A. R. Bodmer and Q. N. Usmani, Nucl. Phys. **A450**, 275c (1986).
[6] A. R. Bodmer and Q. N. Usmani, Nucl. Phys. **A463**, 221c (1987); **A468**, 653 (1987).
[7] Q. N. Usmani, A. R. Bodmer, and Bhupali Sharama, Phys. Rev. C **70**, 061001(R) (2004).
[8] Rita Sinha, Q. N. Usmani, and B. M. Taib, Phys. Rev. C **66**, 024006 (2002).
[9] Q. N. Usmani and A. R. Bodmer, Phys. Rev. C **60**, 055215 (1999).
[10] Th. A. Rijken and Y. Yamamoto, Phys. Rev. C **73**, 044008 (2006), and references therein.
[11] D. E. Lanskoi and T. Yu. Tret'yakova, Sov. J. Nucl. Phys. **49(2)**, 248 (1989).
[12] T. H. Ho and A. B. Volkov, Phys. Lett. **B30**, 303 (1969).
[13] T. H. Ho and A. B. Volkov, Phys. Lett. **B31**, 259 (1970).
[14] J. Žofka and M. Sotona, JINR Report E-4-l, Dubna 1682 (1978).
[15] M. Rayet, Nucl. Phys. **A367**, 381 (1981).
[16] J. Žofka, Czech. J. Phys. **B30**, 95 (1980).
[17] J. Žofka, Czech. J. Phys. **B32**, 321 (1982).
[18] W. H. Bassichis and A. Gal, Phys. Rev. C **1**, 28 (1970).
[19] M. Rayet, Ann. Phys. (NY) **102**, 226 (1976).
[20] D. E. Lanskoy and Y. Yamamoto, Phys. Rev. C **55**, 2330 (1997).
[21] D. E. Lanskoy, Phys. Rev. C **58**, 3351 (1998).
[22] H. Feshbach, in *Proceedings of the Summer Study Meeting on Kaon Physics and Facilities, Brookhaven, 1976*, edited by B. Palevsky, Brookhaven National Laboratory, BNL-50579 (1976), p. 391.
[23] E. Hiyama, M. Kamimura, T. Motoba, T. Yamada, and Y. Yamamoto, Phys. Rev. C **66**, 024007 (2002).
[24] K. Tanida *et al.*, Phys. Rev. Lett. **86**, 1982 (2001).
[25] J. P. Blaizot, Phys. Rep. **64**, 171 (1980).
[26] J. P. Blaizot, J. F. Berger, J. Dechargé, and M. Girod, Nucl. Phys. **A591**, 435 (1995).
[27] Q. N. Usmani, M. Sami, and A. R. Bodmer, in *Proceedings DAE Symposium on Nuclear Physics*, **35B**, 304 (1992), edited by D. R. Chakrabarty and Suresh Kumar.
[28] Q. N. Usmani, M. Sami, and A. R. Bodmer, in *Proceedings of the International Workshop on Codensed Matter Theories*, edited by J. W. Clark, K. A. Shoeb, and A. Sadiq (Nova Science Publishers, Commack, NY, 1994), p. 381.

[29] W. D. Myers and W. J. Swiatecki, Ann. Phys. (NY) **55**, 395 (1969).
[30] W. D. Myers and W. J. Swiatecki, Ann. Phys. (NY) **84**, 186 (1974).
[31] J. Treiner and H. Krivine, Ann. Phys. (NY) **170**, 406 (1986).
[32] J. Dabrowski and H. S. Kohler, Nucl. Phys. **A499**, 453 (1989).
[33] M. Centelles, P. Leboeuf, A. G. Monastra, J. Roccia, P. Schuck, and X. Viñas, Phys. Rev. C **74**, 034332 (2006).
[34] M. Centelles, P. Schuck, and X. Viñas, Ann. Phys. (NY) **322**, 363 (2007).
[35] I. Bombaci and U. Lombardo, Phys. Rev. C **44**, 1892 (1991).
[36] M. Beiner, H. Flocard, N. V. Giai, and P. Quentin, Nucl. Phys. **A238**, 29 (1975).
[37] J. F. Berger, M. Girod, and D. Gogny, Comput. Phys. Commun. **63**, 365 (1991); Nucl. Phys. **A502**, 85c (1989).
[38] R. B. Wiringa, V. G. J. Stoks, and R. Schiavilla, Phys. Rev. C **51**, 38 (1995).
[39] B. S. Pudliner, V. R. Pandharipande, J. Carlson, and R. B. Wiringa, Phys. Rev. Lett. **74**, 4396 (1995).
[40] R. B. Wiringa, V. Fiks, and A. Fabrocini, Phys. Rev. C **38**, 1010 (1988).
[41] A. R. Akmal, V. R. Pandharipande, and D. G. Ravenhall, Phys. Rev. C **58**, 1804 (1998).
[42] S. Shlomo, Tapas Sil, V. Kim Au, and O. G. Pochivalov, Phys. At. Nucl. **69**, 1132 (2006).
[43] O. Bohigas, A. M. Lane, and J. Martorell, Phys. Rep. **51**, 267 (1979).
[44] L. Satpathy, V. S. Uma Maheswari, and R. C. Naya, Phys. Rep. **319**, 85 (1999).
[45] O. Hashimoto and H. Tamura, Prog. Part. Nucl. Phys. **57**, 564 (2006), and references therein; R. Chrien, Nucl. Phys. **A478**, 705c (1988); P. H. Pile *et al*., Phys. Rev. Lett. **66**, 2585 (1991); B. Povh, Prog. Part. Nucl. Phys. **5**, 245 (1980).
[46] H. de Vries, C. W. de Jager, and C. Vries, At. Data Nucl. Data Tables **36**, 495 (1986).
[47] E. G. Nadjakov, K. P. Marinova, and Yu. P. Gangrsky, At. Data Nucl. Data Tables **56**, 133 (1994).
[48] G. Audi, A. H. Wapstra, and C. Thibault, Nucl. Phys. **A729**, 337 (2003).
[49] D. M. Brink and E. Boeker, Nucl. Phys. **A238**, 29 (1975).
[50] D. Gogny, *in Nuclear Self Consistent Fields*, edited by G. Ripka and M. Porneuf (North-Holland, Amsterdam, 1975), p. 333.
[51] H. S. Köhler, Nucl. Phys. **A258**, 301 (1976).
[52] M. Samyn, S. Goriely, M. Bender, and J. M. Pearson, Phys. Rev. C **70**, 044309 (2004).
[53] G. F. Bertsch, B. Sabbey, and M. Uusnakki, Phys. Rev. C **71**, 054311 (2005).
[54] D. J. Millener, C. B. Dover, and A. Gal, Phys. Rev. C **38**, 2700 (1988).
[55] Q. N. Usmani, Nucl. Phys. **A430**, 397 (1980).
[56] G. Alexandar *et al*., Phys. Rev. **173**, 1452 (1968); Sechi-Zorn *et al*., *ibid*. **175**, 1735 (1968).
[57] D. J. Millener, Nucl. Phys. **A691**, 93 (2001).
[58] R. J. Lombard, S. Marcos, and J. Mareš, Phys. Rev. C **51**, 1784 (1995).
[59] S. Stringari, Phys. Rev. Lett. **77**, 2360 (1996).
[60] Jean-Paul Blaizot, RIKEN Rev. No. **23**, 23 (July, 1999).
[61] A. R. Bodmer and Q. N. Usmani, Phys. Rev. C **67**, 034305 (2003).